The formation of complex organic molecules in dense clouds : sweet results from the laboratory

Chuang, K.

1 INTRODUCTION

1.1 INTERSTELLAR MOLECULES AND THEIR COSMOCHEMICAL EVOLUTION

Everything in our daily life, such as the Sun we see, the soil we stand on, the water we drink, and even the molecules we are made of, all of these have had their origin in the interstellar medium (ISM). This highly dilute environment, spaced between stars, consists of ~99% gas and 1% dust by mass (~10^{-12} by number with respect to the element hydrogen). The gas composes ~89% atomic hydrogen, ~9% helium, and ~2% heavier elements. The dust that is typically submicron in size (~ 0.1 μm) comprises iron— or magnesium—bearing silicates, and carbonaceous material (Draine & Lee 1984; Henning & Mutschke 1997). The gas and dust are not homogeneously distributed in space, but rather concentrated in certain regions, known as interstellar clouds. According to the different physical and chemical conditions (density, temperature, visual extinction (A_V), and chemical composition), interstellar clouds can be categorized following three different stages; (1) diffuse clouds, (2) translucent clouds, and (3) dense dark clouds.

In diffuse clouds, the density and temperature are extremely low, i.e., $n_H \approx 10^2$ cm^{-3} and T<80 K, which allows optical and UV-photons from the interstellar radiation field (ISRF), to fully penetrate the cloud, and to intensively irradiate the gas and the dust grains ($A_V \leqslant 1$). The energetic UV-photons dissociate and ionize most molecules into atomic and ionic form. Diffuse clouds are the first stage in complex process ultimately resulting in the formation of new stars and planets. A disturbance, such as a supernova shock, turbulence, cloud-cloud collisions, winds from old stars, outflows from young stars, and on larger galaxy scales spiral density waves, can compress a diffuse cloud. The resulting translucent clouds have a somewhat higher density of ~10^3 cm^{-3}. In this stage, the optical and UV-photons are partially shielded by dust grains ($1 \leqslant A_V \leqslant 5$). Dust temperatures drop to ~15 K. Ionized carbon atoms transfer into their neutral form C and CO molecules in the gas phase (van Dishoeck & Black 1989). When $A_V \geqslant 3$, H_2O ice starts forming through the sequential hydrogenation of atomic and molecular oxygen on grain surfaces (Whittet et al. 1988; Boogert et al. 2015; Wakelam et al. 2017).

Further contraction leads to dark clouds with densities of ~10^{4-5} cm^{-3} ($A_V \geqslant 10$), and the temperature decreases to ~10 K. In this stage, known as the prestellar core phase, most of the gaseous species are in molecular form and they accrete onto the pre-formed H_2O ice mantle at 10 K, with the exception of H_2 and He. This cloud can be maintained for some time by the combination of thermal, turbulent and magnetic pressure, but eventually gravity takes over and the cloud collapses. Initially the cloud stays very cold because the molecules radiate the gravitational energy away, but ultimately the innermost region becomes opaque and warm, i.e., no radiative energy escapes. The core then becomes a protostar in which nucleosynthesis

does not yet happen, but which does emit a continuum of infrared radiation. The entire collapsing object is called a Young Stellar Object (YSO). Due to the conservation of the angular momentum, the rotating spheres of gas and dust can lead to the formation of a protoplanetary disk with bipolar outflows perpendicular to the disk (Shu et al. 1991). The dust and gas in the disk plane will eventually evolve in the formation of planets, their moons and other celestial bodies. When the temperature of the protostar is sufficiently high to initiate nuclear fusion, the new star, 'sun', is born. Depending on its mass, a star can live several billion years. Once it starts running out of fusion material, a number of processes are triggered, resulting in the collapse of the inner core, while the outer layer regions will be expelled as blown away, resulting in a planetary nebula. This fertilizes the ISM with chemically enriched material to be included in a next generation of stars and planets.

1.2 INTERSTELLAR MOLECULES

To date (Spring 2018), astronomical observations have resulted in the identification of some 200 different molecular species in the ISM or circumstellar shells, not including isotopologues and isotopomers, (CDMS:https://www.astro.uni-koeln.de/cdms/molecules), mainly by rotational (radio-astronomy), but also vibrational (infrared), and electronic (UV-VIS) spectroscopy. The list with interstellar molecules comprises various types of species, such as inorganics (e.g., H_2O, CO, CO_2, and NH_3), organics (e.g., CH_4, CH_3OH, and H_2CO), anions (e.g., $C_{2n}H^-$; n = $2-4$), cations (e.g., H_3^+, HCO^+, N_2H^+), unsaturated hydrocarbon chain radicals (e.g., C_nH; n = $2-8$), fullerenes (e.g., C_{60}, C_{70}, and C_{60}^+), and aromatic hydrocarbons (e.g., *c*-C_6H_5CN). Molecular hydrogen, H_2 is the most abundant molecule, at four orders of magnitude higher concentration than the second most abundant species CO. Over the last decades also much has been understood of the involved formation mechanisms that range from reactions in the gas-phase and solid state to gas-grain surface interactions (Herbst & Klemperer 1973; Tielens & Hagen 1982; Garrod et al. 2009; Wakelam et al. 2010; Aikawa et al. 2012; Taquet et al. 2012; Herbst & van Dishoeck 2009; Walsh et al. 2014a,b; Ruaud et al. 2016).

In interstellar clouds, ion-molecule reactions dominate the gas-phase chemistry, and successfully explain the observed abundances of simple hydrocarbons, protonated species, unsaturated species, as well as the relatively high fraction of deuterated species (Herbst 1997; Geballe & Oka 1996; Wootten 1987; Millar et al. 1989). The key processes in the gas-phase are through reactions between ionized species (e.g., H_2^+ produced by cosmic rays interacting with the gas) and neutral molecules (e.g., H_2) to form ions (e.g., H_3^+). H_3^+ can subsequently react with another species "X" resulting in XH^+ through proton transfer. CO^+, via C^++OH, meets H_2 producing HCO^+, which further reacts with an electron giving neutral CO through dissociative recombination. Gas-phase reactions cannot reproduce all the observed abundances, such as the most abundant molecule H_2, fully saturated molecules (e.g., H_2O, NH_3, CH_3OH), lager complex organics, or species only produced in acid-base reactions (e.g., NH_4^+). For this, grain surface reactions and gas-grain interactions are required. The underlying solid-state formation mechanisms have been extensively studied, theoretically, in laboratory studies and through astrochemical models (Tielens & Hagen 1982; D'Hendecourt et al. 1985; Tielens & Allamandola 1987; Charnley et al. 2001; Garrod et al. 2008; Cuppen et al. 2009; Vasyunin & Herbst 2013a; Linnartz et al. 2015; Öberg 2016).

1.2.1 *Formation of icy dust grains*

At low temperatures and sufficiently high densities, the submicron—sized dust grains form a perfect place for gaseous species to accrete, meet, react, and eventually desorb. In translucent and dense dark clouds, the optical and UV extinction is relatively high, and temperature values drop down to $10 - 15$ K. In this temperature regime, atoms and molecules start accreting forming a so-called "ice mantle" (the term ice refers to any species frozen in the solid state). The interstellar ice mantle acts as a molecule reservoir, where the chance of particles to interact is much larger than in the gas phase. Upon reaction, excess energy is released to the surrounding ice, offering a third body (and chemical catalyst) to stabilize new molecules that are formed through exothermic reactions. In dense clouds, the flux of molecular and atomic hydrogen arriving on a dust grain is expected to be $\sim 10^8$ molecules cm^{-2} s^{-1}, and $\sim 10^4$ atoms cm^{-2} s^{-1}, respectively. The accretion of H_2 and H-atoms on a single grain (radius $\sim$0.1 μm) happens about once every 10 seconds, and once a day, respectively. At the low H-atom flux that is realized at 10 K, an H-atom can visit all sites on the grain surface (coverage of 10^6 sites) many times before desorption, or react with another reactant forming new species before the next H-atom impacts. The layers with deposited and produced molecules can be as thick as 0.01 μm (Boogert et al. 2015).

1.2.2 *Interstellar ice composition*

Within the solid state, molecules cannot freely rotate. As a consequence, interstellar ices are usually studied through the infrared (IR) absorption spectrum, monitoring typical vibrational modes. This is realized by observing embedded young stellar objects, or along line of sight to a background star. In the IR, ground based observations are strongly hindered by the Earth's atmosphere, due to polluting H_2O and CO_2 absorptions. Consequently, air-borne and space observations have been used to derive interstellar ice compositions, their chemical environment, abundances, and temperature history (van Dishoeck & Blake 1998). The Infrared Space Observatory (ISO, see Whittet et al. 1996; Gibb et al. 2000, 2004) and the Spitzer Space Telescope (SST, see Boogert et al. 2008; Pontoppidan et al. 2008; Bottinelli et al. 2010; Öberg et al. 2011b) in the range of $2.4 - 200$, and $5 - 35$ μm, respectively, revealed many astonishing ice features which are classified into three different groups; (1) H_2O, CO, CO_2, CH_3OH, NH_3, and CH_4 for secure identification, (2) H_2CO, OCN^-, and OCS for likely identification, and (3) HCOOH, CH_3CH_2OH, CH_3CHO, $HCOO^-$, SO_2, and NH_4^+ for possible identification (see review Boogert et al. 2015).

A typical IR spectrum in the range of $2 - 80$ μm for a massive YSO is shown in Figure 1.1. An interpretation of these astronomical features in terms of molecule identification and environmental conditions, such as ice mixing ratios and ice temperature, is possible because of systematic laboratory investigations of IR spectra of a large number of pure and mixed ices recorded for different temperature settings and ice preparations (Tielens et al. 1991; Hudgins et al. 1993; Gerakines et al. 1995; Baratta & Palumbo 1998; Cuppen et al. 2011; Boogert et al. 2015; Terwisscha van Scheltinga et al. 2017). For example, a comparison between observational (ESO Very Large Telescope and Keck telescope) and laboratory results shows that interstellar ices are partially layered, starting with a H_2O-rich layer and a CO-rich layer coated on top of this H_2O layer (Tielens et al. 1991; Pontoppidan et al. 2003). As solid-state formation schemes are linked to specific molecules, this also means that some species will be more abundant in the water rich and other species in the CO rich environments. This spectroscopic confirmation is fully consistent with the picture of interstellar cloud evolution; in translucent clouds, O (O_2) and H-atoms accrete on a grain surface forming a polar H_2O-rich layer with other minor

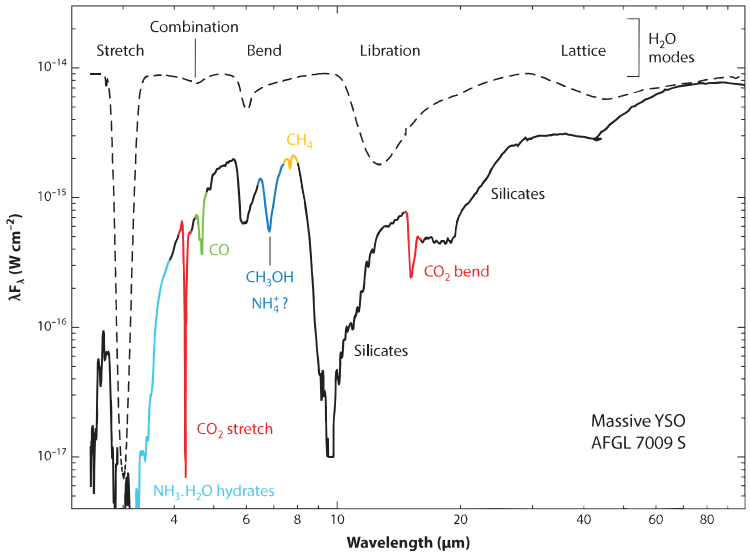

Figure 1.1: The strongest ice and dust features in the massive YSO AFGL 7009S obtained from Infrared Space Observatory (ISO) (Dartois et al. 1998). The figure is taken from Boogert et al. (2015).

hydrogenated species, e.g., NH_3, and CH_4. When the density increases to 10^{4-5} cm^{-3}, the abundant gaseous CO starts dominating the accretion process (Pontoppidan 2006), resulting in an apolar (non-polar) ice layer and offering a reservoir for the formation of complex organic molecules. The observed ice abundances for these different environments are summarized in Table 1.1.

The formation of COMs is linked to the question: does life has its building blocks in space? Observational searches in the mid-infrared (MIR) range, especially at 5 – 10 μm, are essential to complement ice evolution studies and to link laboratory and modeling studies that investigate the formation of organic species on grain surfaces. The James Webb Space Telescope (JWST), with extremely high detection sensitivity, very high spatial and relatively high spectral resolution, will further add to the understanding whether life had a cold start on interstellar dust grains.

1.2.3 *Interstellar COMs: complex organic molecules*

Among the observed interstellar molecules, there are about 50 species that contain six or more atoms and at least one carbon atom. These species are the so-called interstellar Complex Organic Molecules (COMs) (Herbst & van Dishoeck 2009; Herbst 2017). It is important to note that the term 'complex' directly relates to the ISM, as for Earthly conditions most of the interstellar molecules are considered to be rather simple species. Moreover, in this thesis, a more restrictive definition for COMs is used, limiting this class of molecules to species possessing more than six atoms and at least two carbon/nitrogen atoms. As a direct consequence, CH3OH is not regarded to be a COM. The first detections of COMs e.g., CH_3CN, NH_2CHO, CH_3CHO, and CH_3CCH, was in massive (high)–mass star-forming regions, such as Orion and Sgr B, through rotational spectroscopy at 100 – 200 K (Solomon et al. 1971; Rubin et al. 1971; Gottlieb 1973; Buhl & Snyder 1973). However, COM detections are not limited

Table 1.1: Interstellar ice species

		%[H_2O]	
Molecule	Massive YSO	Low-YSO	Comets
Securely identified			
H_2O	100	100	100
CO	$3-26$	$(<3)-85$	$0.4-30$
CO_2	$11-27$	$12-50$	$4-30$
CH_3OH	$(<3)-31$	$(<1)-25$	$0.2-7$
NH_3	~ 7	$3-10$	$0.2-1.4$
CH_4	$1-3$	$1-11$	$0.4-1.6$
Likely identified			
OCN^-	$0.1-0.9$	$(<0.1)-11$	-
OCS	$0.03-0.16$	1.6	$0.1-0.4$
H_2CO	$\sim 2-7$	~ 6	$0.11-1$
Possibly identified			
HCOOH	$(<0.5)-6$	$(<0.5)-4$	$0.06-0.14$
CH_3CH_2OH	$(<0.5)-6$	-	-
$HCOO^-$	$0.3-1$	~ 0.4	-
CH_3CHO	$3.3-11$	-	-
NH_4^+	$9-34$	$4-25$	-
SO_2	$(<0.9)-1.4$	~ 0.2	0.2
PAH	~ 8	-	-
HNCO	$<0.3-0.7$	-	$0.02-0.1$
NH_2CHO	<1.5	-	0.002

Table reproduced from Table 2 and 3 of Boogert et al. (2015)

to high-mass protostars. Meanwhile, a great number of COMs are reported toward low-mass protostars, such as IRAS 16293-2433, NGC1333 IRAS2A, and NGC1333 IRAS4A (Jørgensen et al. 2016; Taquet et al. 2015; Coutens et al. 2015). The interstellar sugar, i.e., glycolaldehyde, which is an important ingredient for ribonucleic acid (RNA) and was first observed in Sgr B2 by Hollis et al. (2000), has now been detected in a solar—mass protostar (IRAS 16293-2422). The formation mechanisms of COMs are traditionally thought to take place on icy grain surfaces, both upon non-energetic and energetic triggers. COM synthesis, for example, can be realized through energetic particles (UV photons, free electrons or cosmic rays) dissociating species to form radicals that can recombine through thermal diffusion. Eventually, the heavier species will desorb into the gas—phase when temperatures reach $\sim 100-150$ K. However, observations showing gaseous COMs in dark cloud and pre-stellar cores challenge the "warm ice" formation scenario (Marcelino et al. 2007; Bacmann et al. 2012; Öberg et al. 2010, 2011a; Cernicharo et al. 2012; Vastel et al. 2014; Jiménez-Serra et al. 2016). Alternative formation channels for explaining the presence of COMs in the early phase of dense cloud have been proposed and discussed in the literature and are at the core of this thesis (Balucani et al. 2015; Fedoseev et al. 2015a; Butscher et al. 2015; Chapter 2; Chapter 3; Chapter 4).

1.3 PHYSICAL AND CHEMICAL PROCESSES IN INTERSTELLAR ICES

In a number of recent studies, partly summarized in this thesis, it has become clear that solid-state chemistry triggered by non-energetic and energetic processes on icy grain surfaces is key in the formation mechanism of hydrogenated species and COMs that contain two, three, or even more carbon elements. Further studies, characterizing the physical and chemical pa-

rameters governing solid-state chemistry, e.g., deposition (binding energy and sticking coefficient), migration (diffusion energy), reaction (activation energy), and desorption mechanism (energy dissipation), under different vacuum, surface material, and cryogenic conditions, provide insight in the actual processes taking place. The details of non-energetic and energetic processes in dense dark clouds are discussed in the next subsections (1.3.1 and 1.3.2). Generally, in surface reactions, radical—molecule and radical—radical reactions typically have small activation barriers or are even barrierless. This makes non—energetic processes - typically atom addition reactions —a possible dominating mechanism resulting in the formation of heavier species at very low temperatures. This also offers a non-thermal low temperature (~10 K) desorption pathway, (Garrod et al. 2007; Minissale et al. 2016; Chapter 6). In addition, the moderate flux of UV-photons or electrons induced by cosmic rays (CR) interacting with hydrogen can trigger energetic processes, to enhance the concentration of radicals in the ice mantle, and to non—thermally desorb the solid-state species into the gas phase. In a later stage of star formation, the interstellar ice will be exposed to higher temperatures and violent UV radiation from the forming (proto)star. More intense chemical reactions can occur, thermally induced, in the 'warm' ice mantle leading to species with high molecular complexity (Schutte et al. 1993; Butscher et al. 2015; Fresneau et al. 2015). Beside sublimation of volatile species due to heat, molecules will be locked in icy grains as these move to the mid-plane of the protoplanetary disk, and become ingredients available for planet and comet formation. Instruments on the *ROSETTA* mission to the comet 67P/Churyumov-Gerasimenko (67P/C-G) studied *in situ* the pristine interstellar ices on the surface and in the coma, and found a remarkable level of molecular complexity, such as glycolaldehyde (interstellar sugar), and even glycine (the simplest amino acid), as well as large amounts of frozen oxygen (Bieler et al. 2015; Le Roy et al. 2015; Goesmann et al. 2015; Altwegg et al. 2016, 2017).

1.3.1 *Non-energetic processes*

Three major processes dominate surface reactions. These follow (1) a Langmuir-Hinshelwood (L-H), (2) an Eley-Rideal (E-R), or (3) a Hot-Atom (H-A) mechanism, as illustrated in Figure 1.2. In the Langmuir-Hinshelwood mechanism, two reactants that are thermally equilibrated on the surface in two different binding sites, diffuse around the available sites and finally meet each other resulting in a new species. In the Eley-Rideal mechanism, one of the reactants directly accretes from the gas phase on top of an absorbed reactant, and the reaction takes place immediately before reaching thermal equilibrium. The Hot-Atom mechanism is somewhat situated between the previous two; the reactant lands on the surface, migrates a considerable distance, and associates with another reactant without thermal equilibrium. The surface is crucial for product synthesis as a way for excess energy dissipation, and the stabilization of the newly formed species.

In dense clouds, H-atom addition, e.g., so-called hydrogenation reactions, are considered to be most prominent due to the substantial abundance of hydrogen in the Universe. The L-H mechanism is the main route to associate two species, since (1) in dense clouds, the temperature of gaseous species and dust grains is ~10 K, and therefore hot-atoms barely exist, and (2) the flux of H-atoms is too low to support reactions through an E-R mechanism. In a laboratory setting, E-R and H-A are hard to distinguish. This is due to the non-negligible temperature difference between H-atom and the absorbed species, as well as the considerable H-atom flux that is normally 8 — 10 orders of magnitude larger in the laboratory than the flux in dense clouds, in order to achieve a comparable fluence in a relatively short time. For this reason it is important to involve modeling simulations, to bridge experiments in the lab with

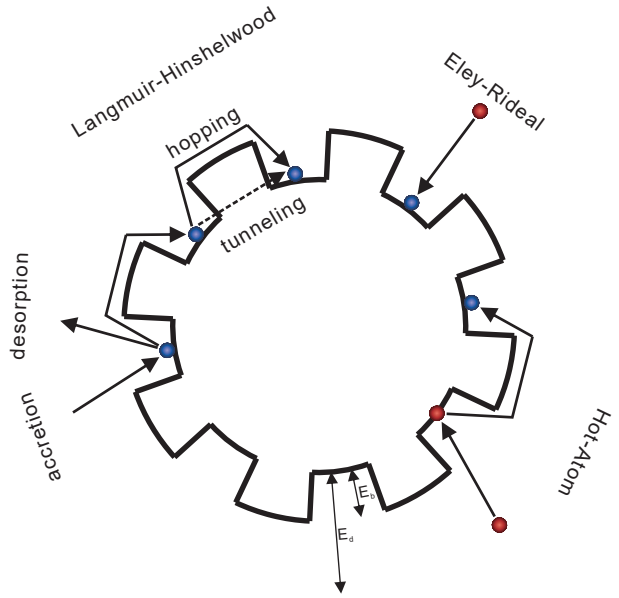

Figure 1.2: Three mechanisms for surface reaction on the grain surface: Langmuir-Hinshelwood, Eley-Rideal, and Hot-atom mechanism. The blue particles are thermalized species and red particles are non-thermalized. E_d is an activation barrier of desorption; E_b is an activation barrier of the diffusion form one surface site to another.

'real' astronomical conditions, compensating for the difference in timescales and to derive the reaction rate constant under interstellar conditions (Cuppen et al. 2009).

Some important hydrogenation routes that result in the formation of abundant interstellar molecules, e.g., H_2, H_2O, CO_2, CH_3OH, and NH_3, are shorty discussed here. H_2 formation is one of the most well studied examples of radical-radical reactions on various surfaces in the laboratory (Islam et al. 2007; Vidali 2013; Wakelam et al. 2017). In dense clouds, two H-atoms accreted on a grain surface diffuse and meet each other forming molecular hydrogen through an L-H mechanism. Molecular hydrogen is also formed through other mechanisms during different stellar evolutionary stages. Due to the extremely low binding energy (~100 K) of accumulating H_2, multilayer H_2 ice is very unlikely to form under interstellar cloud conditions. Newly formed H_2, therefore, will quickly be released into the gas phase. H_2O is the most abundant ice species. The formation of H_2O mainly starts in translucent clouds by means of the interaction between H-atoms and oxygen allotropes, i.e., O, O_2, and O_3, as shown in Figure 1.3 (Ioppolo et al. 2008; Miyauchi et al. 2008; Linnartz et al. 2015). A similar pathway can be applied to explain the solid-state formation of CH_4 and NH_3 (Hidaka et al. 2011; Fedoseev et al. 2015b). CO_2 ice can be formed in different ways. An efficient channel is through the reaction CO + OH, as shown in Figure 1.3. Alternatively, direct addition of atomic oxygen to CO is another possible channel, but with a typically high H/O ratio in dense dark clouds this reaction competes with the barrierless O + H channel that forms the OH radical.

The solid state formation of oxygen-bearing organic ice species, such as CH_3OH, was first proposed by Tielens & Hagen (1982), and confirmed by modeling and laboratory work, as shown in the left panel of Figure 1.3 (Charnley 1997; Cuppen et al. 2009; Chang & Herbst 2012; Hiraoka et al. 1994; Watanabe & Kouchi 2002; Zhitnikov & Dmitriev 2002; Fuchs et al. 2009).

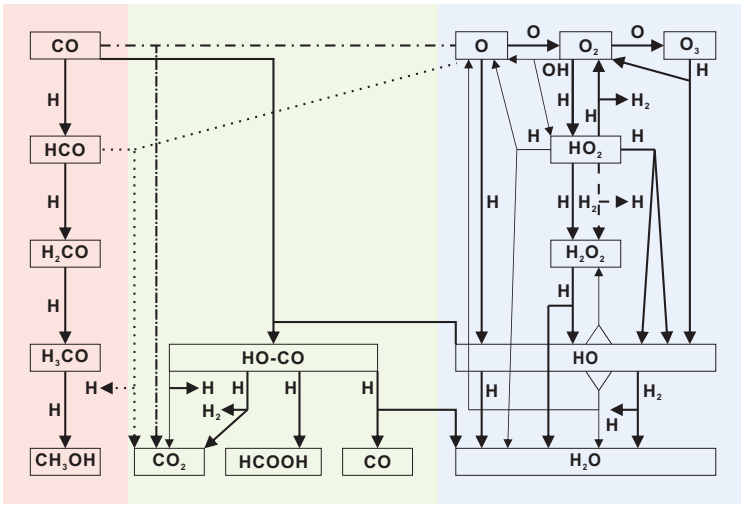

Figure 1.3: A schematic representation of the reaction network for CH_3OH (left), H_2O (right), and CO_2 (middle) on grain surfaces. The figure is taken from Linnartz et al. 2015.

In prestellar cores ($n_H \approx 10^5$ cm^{-3} and T≈10 K), gaseous CO catastrophically freezes out on the grain surface, and reacts with impacting H-atoms through along the sequence:

$$CO \xrightarrow{+H} HCO \xrightarrow{+H} H_2CO \xrightarrow{+H} CH_3O(CH_2OH) \xrightarrow{+H} CH_3OH \quad (1)$$

The first and third H-atom addition reactions, forming HCO, and CH_2OH/CH_3O, have a similar activation energy of ~2400 K, reported in the gas-phase. Later, isotope laboratory studies with D-atoms showed that the deuteration of CO forms similar products, but in the corresponding deuterated form. The derived reaction rate constant for deuteration is about ten times less than the rate constant for hydrogenation indicating that the reaction barrier of H + CO and D + CO takes place through tunneling (Hidaka et al. 2007). Clearly, solid-state reactions may result in H/D abundances that deviate from natural values.

Beside H-atom addition reactions, also H-atom abstraction reactions play an important role (Tielens & Hagen 1982). Laboratory studies demonstrate that the H-D substitution for H_2CO and CH_3OH is through H abstraction reactions, and results in H_2CO-d_n (n = 1 − 2) and CH_3OH-d_m (m = 1 − 3) formation, respectively, as shown in Figure 1.4 (Nagaoka et al. 2005; Hidaka et al. 2009). In this Thesis it is shown that the formation of oxygen-bearing complex organic molecules involves recombination of radicals that are formed both in addition and abstraction reactions in the CO-H_2CO-CH_3OH hydrogenation chain (Woods et al. 2013; Fedoseev et al. 2015a; Chapter 2; Chapter 3). Barrierless radical-radical recombinations on grain surfaces open a new door to form COMs starting from the simple species CO in the very early stages of dense dark cloud formation.

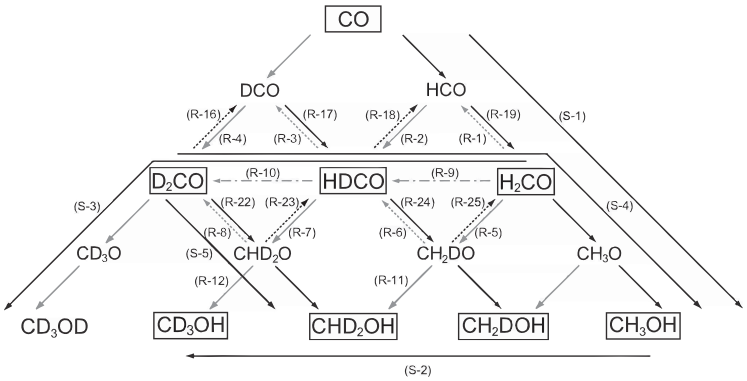

Figure 1.4: Surface reaction network of CO exposed to H and D atoms. The solid arrows refer to for atom addition reactions; the dashed arrows indicate atom abstraction reactions. Molecules in rectangular frame are astronomically observed. The figure is taken from Hidaka et al. (2009)

1.3.2 *Energetic processes*

In dense dark clouds, the interstellar radiation field (ISRF) is blocked by the abundant dust grains as a result of absorption or scattering. However, cosmic rays, i.e., highly energetic particles (proton, charged helium, and heavy metal nuclei), are able to affect the inner dense cloud and interact with gaseous H_2 and dust particles along their path, resulting in (secondary) UV-photons (typically at Ly-α and H_2 emission wavelengths) and electrons. The flux of the CR induced UV field is $(1-10)\times10^3$ photons cm^{-2} s^{-1}, for a CR dissociation rate of $\sim10^{-17}$ s^{-1} (Prasad & Tarafdar 1983; Mennella et al. 2003; Shen et al. 2004). Although the UV-photon (and electron) flux is lower than that of the dominating H-atoms, these energetic particles can easily penetrate the entire ice mantle, and react with accreted molecules that originated from the gas phase, e.g., CO, or new species formed through surface hydrogenation, such as H_2O, CH_4, NH_3 and CH_3OH.

Several laboratory studies have focused on the role of energetic processes, i.e., UV-photons, electrons, X-rays, and protons, and showed the efficient formation of COMs in ice mantles (Greenberg et al. 1995; Bernstein et al. 2002; Muñoz Caro et al. 2002; Meierhenrich 2005; Nuevo et al. 2008; Öberg et al. 2009; Öberg 2016; Modica & Palumbo 2010; Chen et al. 2013; Boamah et al. 2014; Maity et al. 2015; Paardekooper et al. 2016a). In the earlier studies, relatively high energetic fluences, and thick ices containing multiple observed interstellar species were used, and GC-MS analysis of the refractory residue after UV-photon processing led to the discovery of biologically relevant compounds, including various amino acids. In the more recent studies, the focus has been moved on pure, binary, and tertiary ices, to allow a characterization of the involved reactions. Moreover, these studies are all *in situ* without the need to isolate a residual.

1.3.3 *Non-thermal desorption mechanisms*

The astronomical gas-phase observations showing unexpectedly high abundances of simple species and complex molecules ($\sim10^{-8}$—10^{-9} n_H) in dense clouds seem to contradict the concept that at such low temperature (10 K) all species must be frozen out on the grain surfaces, forming ice mantles, except H_2 and He due to their extremely low binding energy. In dense

clouds, the temperature of grain surfaces is too low to sublimate the condensed molecules; thermal desorption is forbidden in this stage. Thus, different non-thermal desorption mechanisms have been proposed to explain the net transfer of frozen molecules from the solid state into the gas phase, such as photo-desorption and reactive desorption.

UV-photon irradiation studies of simple species, e.g., CO, CO_2, H_2O, and CO:N_2 ice mixture, have been investigated and discussed to offer an efficient non-thermal desorption pathway. Broad band UV-light of H/H_2 emissions in a microwave discharge H_2 flowing lamp (MDHL) was used, or narrow-band (but tunable) UV light using a synchrotron source (Öberg et al. 2007; Muñoz Caro et al. 2010; Fayolle et al. 2011; Chen et al. 2014; Fillion et al. 2014; Paardekooper et al. 2016b). However, for molecules like CH_3OH, which is abundantly detected in the gas phase ($\sim 10^{-9}$ n_H), photon-dissociation becomes a dominant channel leading to photo-fragmentation, forming CH_3O, CH_2OH, and CH_3 (Bertin et al. 2016; Cruz-Diaz et al. 2016). The reported upper limit desorption rate, i.e., $<10^{-6}$ molecules photon^{-1}, is too small to substantially transfer CH_3OH into gas phase. It is expected that this also holds for other organic species larger than CH_3OH.

Alternatively, reactive desorption, i.e., desorption following the exothermic formation of species, may contribute to the gas-phase enrichment of both simple molecules, e.g., CO, and complex species, e.g., CH_3OH. Upon formation, excess energy, typically a few eV, can release bound molecules into the gas phase. Up to recently, laboratory studies of reactive desorption of CO-H_2CO-CH_3OH hydrogenation scheme in multi-layered CO-rich interstellar ice analogues are lacking. Therefore, the reactive desorption fraction, i.e., the efficiency of product desorption from the surface after reaction, is usually handled in astronomical models as a free parameter in the range of $0.01 - 0.10$ to account for the steady state gas-phase abundances of simple species observed in dense clouds (Garrod et al. 2007; Vasyunin & Herbst 2013b). Garrod et al. (2007) showed that models including chemical desorption require a reactive desorption fraction of 0.03 to optimally represent the observed gaseous CH_3OH abundances.

All these non-thermal desorption studies, including investigation of exothermic energy dissipation, reactive desorption, photo-absorption cross-sections, and photo-desorption, are crucial to understand how interstellar molecule transfer from solid state to gas phase is influenced by non-energetic and energetic processes (Fayolle et al. 2011; Cruz-Diaz et al. 2014a,b; Fredon et al. 2017). In this thesis, reactive desorption is studied for reactions taking place along the CO hydrogenation chain.

1.4 INTERSTELLAR ICE IN LABORATORY

In this section the experimental setup is described to simulate the processes described above. To comprehensively study the involved processes and to understand the dependency on the physical and chemical processes at play, it is important to experimentally mimic realistic surface scenarios under dense cloud conditions as good as possible. Experiments are therefore performed under ultra-high vacuum (UHV; $\leqslant \sim 10^{-9}$ mbar) and at cryogenic conditions, incorporating both energetic and non-energetic triggers. Simulating interstellar conditions on a much shorter time scale than usual in space is a challenging task for an experimentalist and not only because of experimental limitations; different processes will be at play at the same time and unraveling their relative importance is a time consuming job that is fortunately possible because in the laboratory conditions can be varied very systematically (Watanabe et al. 2007; Henderson & Gudipati 2015). This allows to compare, for example, the competition between ice fragments (i.e., radicals and atoms) and H-atom accretion from the gas-phase (Chapter 4; Chapter 5).

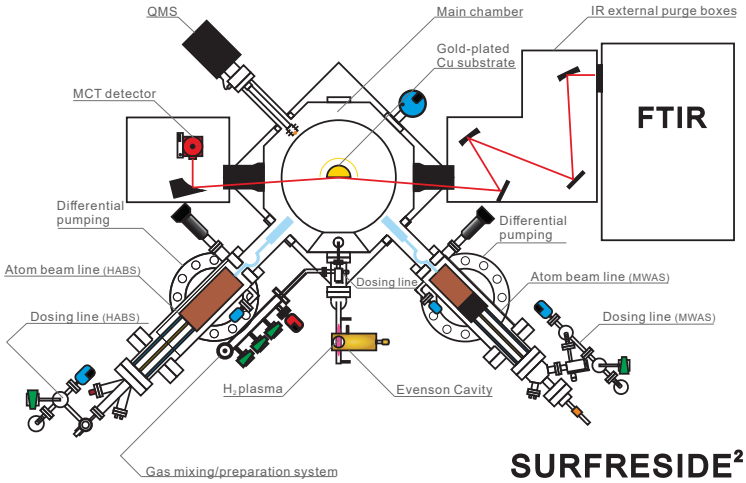

Figure 1.5: Schematic top-view of SURFRESIDE^2. Figure is adapted from Ioppolo et al. (2013).

1.4.1 *Experimental Setup*

The laboratory studies presented in this thesis are performed in the Sackler Laboratory for Astrophysics using SURFRESIDE^2 (Surface Reaction Simulation Device 2), an ultra-high vacuum system fully optimized to study atom addition/abstraction reactions in interstellar ice analogues under dense interstellar cloud conditions. A top-view of the setup is shown in Figure 1.5. This upgraded system is operational since 2012, and has been further extended in the past few years to simulate more sophisticatedly the ice chemistry in environments relevant for interstellar studies. Details are available from Ioppolo et al. (2013). This setup consists of a main chamber and two atom source chambers, which are all differentially pumped to $10^{-10} - 10^{-9}$ mbar (i.e., $\sim 10^{6} - 10^{7}$ cm^{-3}) by turbomolecular pumps and rotary vane vacuum forepumps. At UHV, the residual gas is mainly H_2 with a negligible amount of H_2O contamination on a cold substrate ($\leqslant 4\times10^{13}$ molecules cm^{-2} for 1 hr). A gold-plated copper substrate is centered in the main chamber and cooled by a closed-cycle helium cryostat (Cold-Edge model: CH-204, supported by a Compressor: HC-4), which allows for manipulation of the substrate temperature between 8 and 450 K using resistive heating wire. Two silicon diode thermal sensors (LS-DT-640B CU) installed right behind the substrate and on the second stage of the cold finger are used to monitor the temperature with 0.5 K absolute accuracy.

Two atom beam lines, incorporated in separate differentially pumped vacuum chambers, are connected with UHV shutter valves to the main chamber at angles of 45 degree in order to study different atom addition/abstraction reactions based on different atom generation methods; (1) Hydrogen Atom Beam Source (HABS, Dr. Eberl MBE-Komponenten GmbH, see Tschersich 2000) producing H- or D-atoms by thermal (2100 K) cracking of precursor H_2 and D_2 through a tungsten filament, and (2) Microwave Atom Source (MWAS, Oxford Scientific Ltd, see Anton et al. 2000) capable of producing H-atoms, D-atoms, and other atoms, e.g., O-, N-atoms, and various radicals (like OH) using a microwave discharge (275 W at 2.45 GHz). A nose-shape quartz pipe is placed along the exit path of both beam lines to efficiently quench and thermalize excited atoms and non-dissociated molecules through multiple collisions with

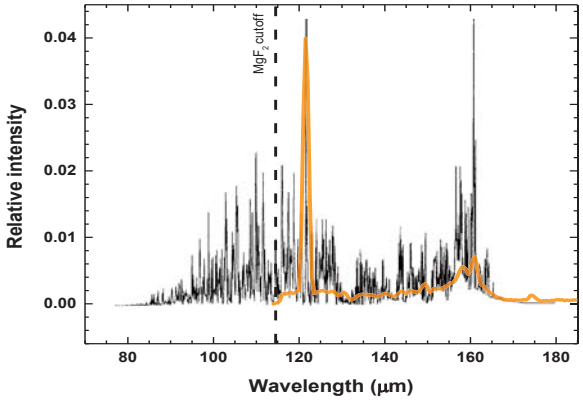

Figure 1.6: UV spectrum (yellow) of the MDHL used in this thesis, which is obtained from Ligterink et al. (2015). The background line (black) is the calculated spectrum of UV photons induced by CR interacting with H_2 molecules in dense clouds, which is obtained from Gredel et al. (1989). The MgF_2 window cutoff is indicated (dashed line).

the walls of the pipe. This quartz pipe also shields the ice sample from UV light ($\lambda \leqslant 200$ nm) generated in the MWAS plasma. Typical atomic beam line fluxes vary (depending on the precursor). Typical H-fluxes are in the range $\sim(1-10)\times10^{12}$ atoms cm^{-2} s^{-1}, and can be simultaneously operated to further increase the H-atom flux.

UV-photons generated by a Microwave Discharge Hydrogen-flow Lamp (MDHL) are guided through an MgF_2 window, and directed on the substrate at normal incidence. The lamp is mounted in between the two atomic beam lines. The customized quartz lamp is 'F' shaped, ~1.3 cm in diameter and ~20.0 cm in length, and combined with a commercial Evenson coaxial Cavity (Opthos). The distance between the UHV sealed MgF_2 window and the substrate is about 30 cm. Without a collimating tube, the UV-beam spot covers the entire substrate area (2.5×2.5 cm^2). The microwave power generator (Sairem-GMS200W, 2.45 GHz) is used to discharge H_2 flowing gas at a pressure of ~1 mbar, generating H_2 plasma and UV light. In Figure 1.6, the UV spectrum ranging between 114 and 180 nm is shown to consist of a main peak at 121.6 nm (Ly-α, ~33% of the total flux) and a series of other peaks between 155 and 165 nm (H_2 emission, ~20% of the total flux) superposed on a broad continuum (~47% of the total flux). The total UV flux is estimated to be $\sim6\times10^{12}$ photons cm^{-2} s^{-1}. Details are available in Ligterink et al. (2015).

Gaseous molecules are prepared in an oil-free gas-mixing/preparation high vacuum ($\leqslant10^{-5}$ mbar) system, which is pumped by a turbomolecular pump backed with a scroll forepump, and stored in two separate reservoir dosing lines. The dosing pressure is monitored by a mass independent gauge in the range of mbar to bar. These vapor species are introduced into the main chamber through one of two capillary tubes controlled by high-precision leak valves, such that they deposit onto the pre-cooled substrate under an angle of +22° (or -22°) from the surface normal. The typical deposition pressure is in the range of $\sim10^{-10}-10^{-8}$ mbar, and ices are grown with sub-monolayer precision in thickness ranges from few ML to several tens of ML. Here 1 monolayer (ML) is defined to be 1×10^{15} molecules cm^{-2}.

Two different ice grows techniques are commonly applied in the experiments described in this thesis; pre-deposition and co-deposition. In the pre-deposition experiments, molecules are

first deposited on the pre-cooled substrate resulting in a pre-grown ice sample before atoms or UV-photons start interacting. Once the ice is bombarded with atoms and/or irradiated with UV-photons, the kinetics of the pre-deposited species and the newly formed products can be obtained. These time-resolved data can be fitted with rate equations to determine the chemical characteristics, e.g., reaction rates and activation energy. In the atom addition/abstraction experiments, the penetration depth is limited to only the upper layers of the pre-deposited ice leading to relative low formation yields. Moreover, the active intermediate radicals formed during the chemical reactions are quickly converted into stable products.

In the co-deposition experiments molecules and atoms (and UV photons) are simultaneously deposited onto the pre-cooled substrate with a specific deposition-flux calibrated in advance. This technique has the ability to study various ratios between the molecular reactants and the atomic species simulating the different ISM density (flux) conditions. Moreover, co-deposition experiments are more representative of the actual processes taking place under dense cloud conditions, where atoms and molecules continuously adsorb onto dust grains. Matrix techniques can be exploited in co-deposition experiments using overabundant molecule depositions to preserve the intermediate radical products, which generally recombine immediately with incoming atoms through barrierless reactions. In this case, the final yield of products is proportional to the co-deposition time, resulting in a more secure identification of the analytical methods used.

1.4.2 *Analytical techniques*

RAIRS: The ice composition and abundance are monitored in situ by means of Reflection-Absorption InfraRed Spectroscopy (RAIRS) using the external IR path from a Fourier Transform Infrared Spectrometer (FTIR; Agilent Technologies Cary 600 Series), and a Mercury Cadmium Telluride (MCT) detector cooled by liquid nitrogen. The IR absorbance spectrum is obtained by taking the common logarithm of the ratio of substrate and ice sample single-beam spectra, i.e., $Abs(\nu) = \log(I_{\text{substrate}}(\nu)/I_{\text{sample}}(\nu))$, which covers the range of $4000 - 700$ cm^{-1} typically with 1 cm^{-1} resolution. As RAIR spectra are continuously recorded, these allow to monitor changes compared with the spectrum for the initially deposited and unprocessed parent species; this allows not only to investigate which species are formed, but also how effectively this process takes place. The icy constituents are identified by their characteristic vibrational modes that are directly connected to different functional groups. The vibrational modes shift when isotopes are used. In general, RAIRS has a higher sensitivity than transmission IR spectroscopy, because (1) the geometry of the IR path in the ice is at least two times longer than in transmission, i.e., the incident sample path before reaching the substrate and the reflecting sample path after hitting the substrate, and (2) the glancing angle $\sim 10^\circ$ to the substrate plane) of IR light enhances the p-polarized electric field at the gold surface resulting in higher sensitivity. It should be noted, though, that the reported IR band strengths available from the literature are generally derived from transmission experiments and these cannot be directly used to quantify RAIR data.

In order to overcome this issue, (setup-specific) RAIR band strengths need to be determined. Therefore, experiments have been performed to separately derive the RAIR band strength values for the most commonly studied species in this Thesis, i.e., CO, H_2CO, and CH_3OH, by using the laser interference technique. A HeNe laser beam hits the gold-plated substrate, at an incident angle of $\sim 3^\circ$ with respect to the surface normal incidence, and the reflecting laser beam intensity is monitored by a photodiode. Simultaneously, the pure ice is introduced onto

the pre-cooled substrate forming ice layers in a constant deposition rate over time. For pure ice, the absolute column density is calculated (molecules cm^2) with the equation:

$$N = \frac{d \cdot \rho \cdot N_a}{M} \tag{2}$$

where d is the thickness of ice in cm, ρ is the density in g cm^{-3}, N_a is Avogadro's constant (6.022×10^{23} mol^{-1}), and M is the molar mass of the species. The ice thickness, d, is experimentally determined by laser refractive interference:

$$d = \frac{k \cdot \lambda \cdot 10^{-7}}{2n \cdot \cos(\theta_f)} \tag{3}$$

where λ = 632.8 nm is the HeNe laser wavelength, n is the refractive index of a specific ice, θ_f=3° is the angle of refraction in the ice in degrees and k is the number of involved fringes (Hollenberg & Dows 1961; Westley et al. 1998). The ice growth on the substrate is monitored by RAIRS for the first few minutes (Figure 1.7 right-hand panel) before RAIR signal saturation. To keep a constant deposition rate for the entire measurement (~hours), a relatively high gas sample pressure is used in the gas-mixing and dosing reservoir lines. The IR absorbance area obtained from the integration of the IR signal is correlated to the absolute column density derived from the laser interference pattern (Figure 1.7 left-hand panel). The correlation is described by the modified Beer-Lambert Law:

$$N = \frac{\log 10 \cdot \int Abs(\nu)\, d(\nu)}{A'} \tag{4}$$

where $Abs(\nu)$ is the IR absorbance intensity, and *A'* is the RAIR band strength value. By linear fitting the data (middle panel Figure 1.7), the *A'* RAIR value can be derived for all relevant modes of the involved molecules. The band strength for CO (2142 cm^{-1}), H_2CO (1497 cm^{-1}), and CH_3OH (1030 cm^{-1}) is derived as: $(5.2\pm0.3)\times10^{-17}$, $(3.2\pm0.3)\times10^{-17}$, and $(7.1\pm0.6)\times10^{-17}$ cm $molecule^{-1}$, respectively.

The identification of specific molecules in RAIR spectra is based on the full ensemble of fingerprint features. Typically, the larger the molecule, the larger the number of vibrational modes that can be seen, and the more specific a functional group, the easier is an unambiguous identification. For example, glycolaldehyde (GA, CH_2OHCHO) contains a hydroxymethyl (-CH_2OH) and an aldehyde (-CHO) group, showing very strong O-H, C-O, and C=O stretching vibration modes at ~3340, ~1750, and ~1110 cm^{-1}, respectively. When bands with these wavelengths are found with SURFRESIDE^2, comparable to molecular fingerprints available from literature, it is very likely that glycolaldehyde is present in the ice. However, it should be noted that in the case that GA is formed in the ice, e.g., upon hydrogenation of CO-ice, it is possible that other molecules with similar functional groups are formed as well, yielding spectra with similar features.

This is part of the discussions in Chapter 2; CO hydrogenation experiments not only give glycolaldehyde, but also yield isomeric species, e.g., methyl formate (MF, CH_3OCHO), and the fully hydrogenated species, e.g., ethylene glycol (EG, $CH_2(OH)CH_2OH$). In this case, the hydroxymethyl (-CH_2OH) and the aldehyde (-CHO) groups are not represented by glycolaldehyde alone, so this complicates the qualitative species identification and quantitative abundance estimation (Figure 1.8). The use of isotopically labeled precursors may help in the identification, but it is also possible to use a complementary detection method.

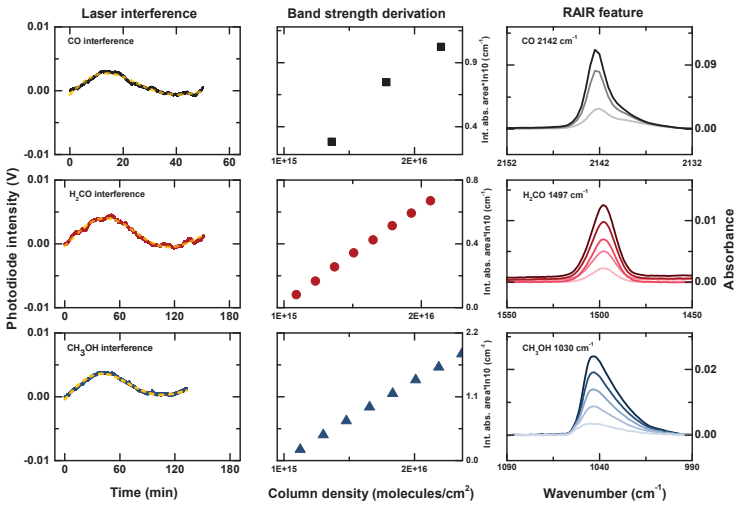

Figure 1.7: Left: typical examples of the obtained interference fringes as function of time and their corresponding sinusoidal fittings (yellow dashed line) deposition of pure CO, H_2CO, and CH_3OH. Right: the RAIR absorbance feature different times for deposited CO (2142 cm^{-1}), H_2CO (1497 cm^{-1}), and CH_3OH (1030 cm^{-1}). Middle: the integrated absorption as a function of column density of each species for the first few minutes of deposition.

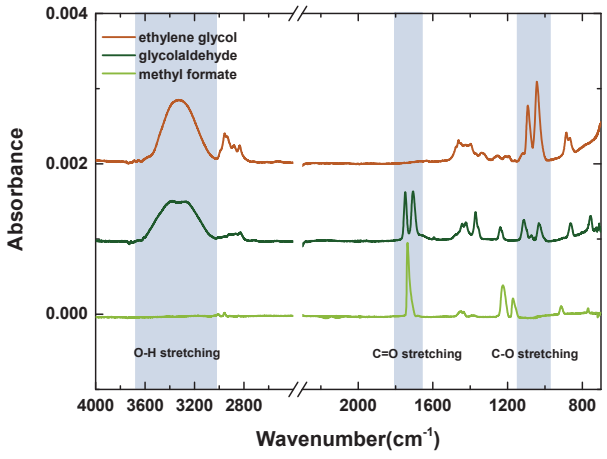

Figure 1.8: IR absorbance spectra of methyl formate, glycolaldehyde, and ethylene glycol in the range of $4000 - 700$ cm^{-1}.

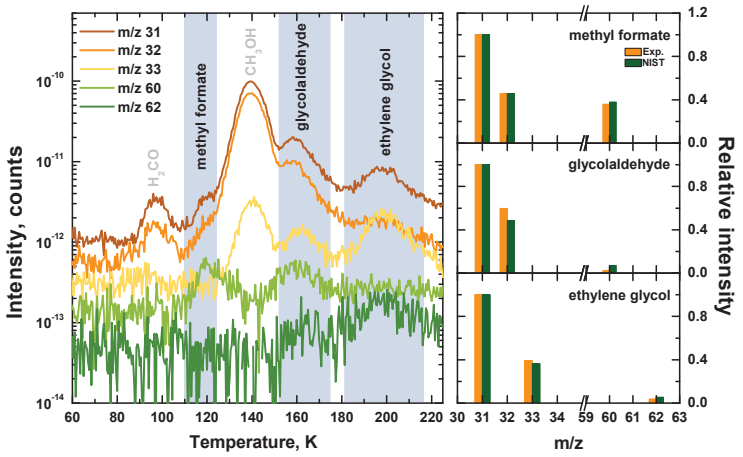

Figure 1.9: Left: TPD mass spectra obtained from a codeposition experiment of H_2CO and H-atoms. The thermal desorption temperatures of methyl formate (*m/z* = 31, 32, and 60), glycolaldehyde (*m/z* = 31, 32, 33, and 60), and ethylene glycol (*m/z* = 31, 33, and 62) are at 120, 160, and 180 K, respectively. Right: comparison of the fragmentation patterns of these COMs with the corresponding NIST[1.1] database.

TPD: During a Temperature Programmed Desorption (TPD) experiment an ice sample, which consists of initially deposited species and newly formed products, is linearly and slowly heated to a preset (high) temperature value, typically with a rate of the order of $1-10$ K min^{-1}. At specific temperatures specific molecules can thermally desorb in the gas phase and this is recorded sensitively by Quadrupole Mass Spectrometry (QMS; MKS Microvision-plus). In the QMS desorbed species are ionized by electrons, which are emitted from a hot filament on the tip of the QMS. The ionized molecules are accelerated and guided into the quadrupole mass filter, which consists of four cylindrical rods oppositely connected to RF voltage with a DC offset voltage in two pairs. Only the ions with certain mass-to-charge ratio (m/z) can reach the detector for a given voltage ratio, and the other ions with different m/z will eventually collide with rods before detection. Two types of detectors can be used in the used QMS for different sensitivities: (1) a Faraday detector for high ion intensity, and (2) a Channel Electron Multiplier (CEM) for trace ion signals ($\gtrsim 5\times10^{-14}$ mbar).

The desorption temperature for each species is another characteristic that depends on the species' binding energy to the surface. Therefore, measuring this characteristic offers a complementary tool to distinguish reaction products that share very similar functional groups. For example, in Figure 1.9, the MF, GA, and EG desorption peaks are located at 120, 160, and 180 K, respectively, in the mass spectrum using the TPD experiment.

The electrons emitted from the ionizing source have an energy of 70 eV, which is sufficient to break COMs, resulting in typical mass fragmentation patterns. This mass fragmentation

[1.1] NIST Mass Spec Data Center, S.E. Stein, director, 'Mass Spectra' in NIST Chemistry WebBook, NIST Standard Reference Database Number 69, Eds. P.J. Linstrom and W.G. Mallard, National Institute of Standards and Technology, Gaithersburg MD, 20899, http://webbook.nist.gov.

pattern offers another fingerprint for each species due to the different molecular structures that correspond with different binding energies. For example, in the right panel of Figure 1.9, the mass fragmentation for MF, GA, EG from a H_2CO hydrogenation experiment is in agreement with the NIST database values. Normally, three typical mass fragments, that is, the total molecular weight, the most abundant signal, and a unique mass, are chosen in order to make a confident species identification.

Under sufficient gas pumping speed, the recorded QMS signal (I(t)) for the selected m/z is proportional to the species desorption rate (dN/dt), and can be described by the Polanyi-Wigner equation:

$$I(\mathrm{t}) \propto dN/dt = \nu(\mathrm{N},\mathrm{T}) \cdot N^{n} \exp\left(\frac{-E_{\mathrm{des}}(\mathrm{N},\mathrm{T})}{k_{\mathrm{b}}T}\right) \tag{5}$$

where ν is the pre-exponential factor, N is the surface coverage, n is the kinetic desorption order, E_{des} is the activation energy for desorption, k_{B} is the Boltzmann constant, and T is the surface temperature. This equation is perfect for describing 'pure' species desorption behavior on surfaces, and allows to derive binding energies for various surfaces (Brown & Bolina 2007; Fayolle et al. 2016). However, in most of the experiments described in this thesis, interstellar ice analogues are 'dirty', containing multiple species in the ice mantle and this leads to more than one binding energy value. Moreover, volatile species may exhibit multiple desorption peaks from co-desorbing with less-volatile species. Therefore, it is not trivial to accurately derive species abundances by fitting TPD peaks in the mass spectrum using equation (5). However, the area of the desorption peak obtained from integration of the QMS signals (I(t)) over time is representative of the species' abundance (N) on the surface. This can be used as a tool to quantify branching ratios for each of the newly formed products.

Care needs to be taken when analyzing the peak area for a given m/z, since this is dependent on several factors: (1) the electronic ionization cross-section (σ^{+}*(mol)*) as a function of energy, which is available for most stable molecules in the literature, (2) the fraction of ionized molecules with charge z (I_{F}*(z)*), which is unity when z = 1, (3) the fraction of mass fragmentation (F_{F}*(m)*), which is available in the literature, and (4) the mass sensitivity (*S(m/z)*), which is setup dependent, as shown in Figure 1.10. The species abundance can be estimated by carefully calibrating the above factors using the equation (Martín-Doménech et al. 2015):

$$N(\mathrm{molecule}) = k_{\mathrm{QMS}} \cdot \frac{A(\mathrm{m/z})}{\sigma^{+}(\mathrm{molecule}) \cdot I_{\mathrm{F}}(\mathrm{z}) \cdot F_{\mathrm{F}}(\mathrm{m}) \cdot S(\mathrm{m/z})} \tag{6}$$

where k_{QMS} is the proportionality constant, which is independent of the species assuming relatively constant pumping speed for all formed products, and need to be independently measured using other techniques. For the relative abundance, it can be derived by the equation:

$$\frac{N_1(\mathrm{molecule1})}{N_2(\mathrm{molecule2})} = \frac{A_1(\mathrm{m/z})}{A_2(\mathrm{m/z})} \cdot \frac{\sigma_2^{+}(\mathrm{molecule2}) \cdot I_{\mathrm{F2}}(\mathrm{z}) \cdot F_{\mathrm{F2}}(\mathrm{m}) \cdot S_2(\mathrm{m/z})}{\sigma_1^{+}(\mathrm{molecule1}) \cdot I_{\mathrm{F1}}(\mathrm{z}) \cdot F_{\mathrm{F1}}(\mathrm{m}) \cdot S_1(\mathrm{m/z})} \tag{7}$$

The TPD experiments thus give a second complementary tool to further constrain the formation of surface reaction products. Obviously, TPD cannot probe species at the temperatures for which the reactions take place. Moreover, during the heating, additional surface reactions could happen. Ice destruction is an intrinsic property of TPD. In many of the experiments that are described in this thesis, RAIRS and TPD are applied simultaneously.

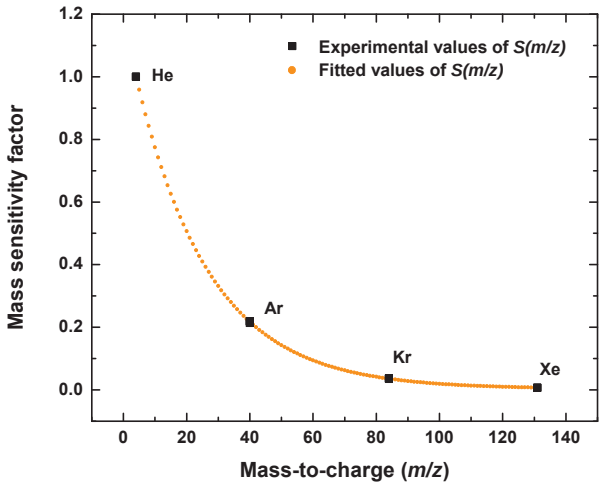

Figure 1.10: QMS detection sensitivity for different mass channels obtained from noble gas calibration experiments.

1.5 THIS THESIS

Interstellar ice mantles consist of simple molecules, e.g., CO, accreting from the gas phase, and of complex species, e.g., CH_3OH and COMs (likely), formed on dust grains. To understand interstellar ice evolution, complementary approaches, i.e., astronomical observations, theoretical/astrochemical models, and laboratory studies, are needed.

The motivation of this thesis is to have a more comprehensive picture of the interactions of CO-hydrogenation products with abundant H-atoms and moderate UV-photons on the grain surfaces under dense cloud conditions. The recent gas-phase discovery of COMs at low temperatures challenges the conventional COM formation scenarios where CH_3OH undergoes intensive UV-photon irradiation, CR bombardment, and 'warm' ice chemistry forming complex organics in the gravitationally collapsing stage. The primary goal of this thesis is to understand how simple solid-sate species transform to COMs without such energetic processes focusing on the CO catastrophically freeze-out stage at temperatures as low as 10 K and to explain the 'cold' COM detections. Moreover, the net transfer of the newly formed species, especially partially or fully hydrogen saturated molecules on the grain surfaces, into the gas phase through non-thermal desorption is currently unconstrained, and is a free parameter in astrochemical models. To this end, experimental studies systematically investigate CO ice hydrogenation, and expand our understanding of the CO-H_2CO-CH_3OH formation network to more complex organics, which contain two, three or even more carbon atoms, such as glycolaldehyde (an interstellar sugar), ethylene glycol, and glycerol (sugar alcohol). The interactions of CO with other interstellar relevant species, e.g., NO and H_2, under moderate UV irradiation are experimentally studied to address the formation of CN-bearing, and of H_nCO ($n \geqslant 1$) species in dense clouds. The utilization of SURFRESIDE^2, an UHV and cryogenic setup in the Sackler Laboratory for Astrophysics, makes it possible to explore molecular complexity and to understand details of the physical/chemical properties on icy grain surfaces. The ex-

perimental findings are summarized below.

Chapter 2 focuses on the formation of oxygen-bearing complex organic molecules, e.g., methyl formate ($HC(O)OCH_3$), glycolaldehyde ($HC(O)CH_2OH$) and ethylene glycol ($H_2C(OH)CH_2OH$), upon hydrogenation and without the influence of energetic particles (e.g., UV-photons and electrons) or embedded energy source under dense dark cloud conditions. The solid-state synthesis mechanisms are realized by the recombination of the intermediate radicals, i.e., HCO, CH_2OH, and CH_3OH, which are produced in the hydrogenation scheme of CO-H_2CO-CH_3OH. We confirm that the interaction of H_2CO with H-atoms not only leads to the hydrogenated species, i.e., CH_3OH, but also results in dehydrogenated species, i.e., CO, through HCO radical. A similar mechanism is also found in abstraction reactions involving CH_3OH to form H_2CO. The simultaneous forward (addition) and backward (abstraction) reactions of stable molecules enhance the lifetime of active radicals on grain surfaces compared to previous assumptions, which consider addition reactions only. The experimental findings unambiguously prove complex organic molecule formation during the early phase of the catastrophic CO freeze-out stage and without the need of UV photolysis or cosmic ray bombardment. The solid-state COM formation network is proposed.

Chapter 3 aims to extend the COM formation network presented in Chapter 2 to three-carbon oxygen-bearing species. Under prestellar core conditions, CO hydrogenation is the dominant pathway leading to H_2CO and CH_3OH formation through successive H-atom addition reactions. The recombination of intermediate radicals with single- and double-carbon containing backbones is experimentally demonstrated to explain the formation of biologically relevant compounds, e.g., glyceraldehyde ($HOCH_2CH(OH)$-CHO), a three-carbon simple sugar, and glycerol ($HOCH_2CH(OH)$-CH_2OH), a three-carbon sugar alcohol. The three-carbon sugar plays a key role in energy transfer in living organisms, and the three-carbon sugar alcohol is an important ingredient for membranes of modern living cells. The proposed formation mechanisms have much potential to form complex sugar alcohols and sugars, which can be delivered by comets or other celestial bodies to planets. The resulting reaction scheme can be further extended to form even larger COMs.

Chapter 4 presents the first systematic experimental study that compares quantitatively hydrogenation and UV-induced reactions as well as their cumulative effect in interstellar relevant CO:CH_3OH=4:1 ice analogues. We focus on three COMs, i.e., methyl formate ($HC(O)OCH_3$), glycolaldehyde ($HC(O)CH_2OH$) and ethylene glycol ($H_2C(OH)CH_2OH$), which are most commonly produced in '(non-)energetic' processes. In the pure hydrogenation experiments, the derived abundances and the abundance fractions are dependent on the ratio of H-atoms/CO:CH_3OH and on the accretion rate of the involved species. The abundance fractions for methyl formate: glycolaldehyde: ethylene glycol are $0{:}(0.2-0.4){:}(0.8-0.6)$ for pure hydrogenation, and 0.2:0.3:0.5 for UV involving experiments. In experiments where both hydrogenation and UV irradiation are applied, the overall absolute yields drop to 50% of those found in the pure UV experiments. However, the COM abundance fractions are identical to the fractions in the pure UV experiments. The COM ratios obtained from the laboratory findings can be used as a diagnostic tool to derive the chemical origin of these species. The GA/EG ratios in the laboratory ($0.3-1.5$) compare well with observations toward various comets and solar-mass protostars suggesting a solid-state formation pathway.

Chapter 5 presents the formation of N-C bearing species obtained from the sequence of NO:CO:H-atom accretion and UV-photon irradiation as well as the simultaneous codeposi-

tion of NO:CO:H-atoms and UV irradiation on grain surfaces. Ice mixtures of NO and hydrogenated CO ices, i.e., comprising H_2CO and CH_3OH, are studied. The UV-irradiation results in NH_2 through photodissociation of NH_2OH, which is the main product of NO hydrogenation. The NH_2 radical plays a key role in the formation of species with an N-C bond, such as HNCO, OCN^-, and NH_2CHO. The formation scheme of N-C bearing species is proposed, and the astronomical implications are discussed.

Chapter 6 presents the reactive desorption fraction of the species along the CO-H_2CO-CH_3OH hydrogenation scheme under prestellar core conditions. The net transfer of solid-state species into the gas phase at very low temperatures, i.e., for settings in which all molecules should be condensed on the grain surface, is experimentally triggered through exothermic reactions with H-atoms in the laboratory. The reactive desorption efficiency for the overall hydrogenation network is derived by precisely measuring the solid-state element carbon budget at $10-14$ K. This results in an upper limit of 0.24 ± 0.02. The corresponding effective desorption fraction for each hydrogenation step and for each H-atom induced reaction (i.e., addition and abstraction) is $\leqslant 0.07$ and $\leqslant 0.02$, respectively. These values favor the lower range of the reactive desorption efficiencies of $0.01-0.10$, which are currently used as a free parameter in astrochemical models.

Chapter 7 investigates whether additional hydrogenation events can take place upon UV irradiation of a CO:H_2 ice mixture under prestellar core conditions. The experimental findings show unambiguously that hydrogenated species, e.g.., HCO and H_2CO, are formed after UV-irradiation on the pre-deposited CO:H_2 ice mixture. A possible formation mechanism is discussed, through a reaction between photo-excited CO and H_2 molecules resulting in HCO and free H-atoms. Moreover, the newly formed H-atoms can further react with CO along a regular addition step. The HCO production shows a strong temperature dependence for the studied $8-20$ K temperature range, which is directly linked to the H_2 sticking coefficient. Isotope experiments in a CO:D_2 ice mixture present a similar trend for the temperature-dependent DCO formation rate, but the overall DCO production efficiency only reaches $\leqslant$25% of the HCO yield at 8 K. Clearly, UV-photon induced hydrogenation enriches interstellar ices with HCO radicals that can further react with other radicals or molecules ultimately also increasing the formation efficiency of COMs. The astrochemical implications are discussed.

The main take-home massage of this thesis is that the building blocks of life are already formed on the grain surfaces at low temperatures before the emerging of the protostar. In dense clouds, the chemical complexity of non-energetic processes is beyond our imagination. The two scenarios of COM formation, i.e., non-energetic and energetic processes, do not conflict each other. Moreover, their product fractions offer a diagnostic potential to derive the formation origin of COMs in different star evolutionary stages. It is therefore expected the upcoming JWST with high spectral resolution and detection sensitivity at mid-infrared wavelengths will greatly increase our knowledge of the interstellar COM evolution from dense cloud to solar system.

BIBLIOGRAPHY

Aikawa, Y., Wakelam, V., Hersant, F., Garrod, R. T., & Herbst, E. 2012, Astrophys. J., 760, 40
Altwegg, K., Balsiger, H., Bar-Nun, A., et al. 2016, Science Advances, 2, e1600285
Altwegg, K., Balsiger, H., Berthelier, J. J., et al. 2017, Mon. Not. R. Astron. Soc., 469, S130
Anton, R., Wiegner, T., Naumann, W., et al. 2000, Review of Scientific Instruments, 71, 1177

Bacmann, A., Taquet, V., Faure, A., Kahane, C., & Ceccarelli, C. 2012, Astron. Astrophys., 541, L12
Balucani, N., Ceccarelli, C., & Taquet, V. 2015, Mon. Not. R. Astron. Soc., 449, L16
Baratta, G. A. & Palumbo, M. E. 1998, Journal of the Optical Society of America A, 15, 3076
Bernstein, M. P., Dworkin, J. P., Sandford, S. A., Cooper, G. W., & Allamandola, L. J. 2002, Nature, 416, 401
Bertin, M., Romanzin, C., Doronin, M., et al. 2016, Astrophys. J. Lett., 817, L12
Bieler, A., Altwegg, K., Balsiger, H., et al. 2015, Nature, 526, 678
Boamah, M. D., Sullivan, K. K., Shulenberger, K. E., et al. 2014, Faraday Discussions, 168, 249
Boogert, A. C. A., Gerakines, P. A., & Whittet, D. C. B. 2015, Ann. Rev. Astron. Astrophys., 53, 541
Boogert, A. C. A., Pontoppidan, K. M., Knez, C., et al. 2008, Astrophys. J., 678, 985
Bottinelli, S., Boogert, A. C. A., Bouwman, J., et al. 2010, Astrophys. J., 718, 1100
Brown, W. A. & Bolina, A. S. 2007, Mon. Not. R. Astron. Soc., 374, 1006
Buhl, D. & Snyder, L. E. 1973, in Molecules in the galactic environment
Butscher, T., Duvernay, F., Theule, P., et al. 2015, Mon. Not. R. Astron. Soc., 453, 1587
Cernicharo, J., Marcelino, N., Roueff, E., et al. 2012, Astrophys. J. Lett., 759, L43
Chang, Q. & Herbst, E. 2012, Astrophys. J., 759, 147
Charnley, S. B. 1997, Mon. Not. R. Astron. Soc., 291, 455
Charnley, S. B., Rodgers, S. D., & Ehrenfreund, P. 2001, Astron. Astrophys., 378, 1024
Chen, Y.-J., Chuang, K.-J., Muñoz Caro, G. M., et al. 2014, Astrophys. J., 781, 15
Chen, Y.-J., Ciaravella, A., Muñoz Caro, G. M., et al. 2013, Astrophys. J., 778, 162
Coutens, A., Persson, M. V., Jørgensen, J. K., Wampfler, S. F., & Lykke, J. M. 2015, Astron. Astrophys., 576, A5
Cruz-Diaz, G. A., Martín-Doménech, R., Muñoz Caro, G. M., & Chen, Y.-J. 2016, Astron. Astrophys., 592, A68
Cruz-Diaz, G. A., Muñoz Caro, G. M., Chen, Y.-J., & Yih, T.-S. 2014a, Astron. Astrophys., 562, A119
Cruz-Diaz, G. A., Muñoz Caro, G. M., Chen, Y.-J., & Yih, T.-S. 2014b, Astron. Astrophys., 562, A120
Cuppen, H. M., Penteado, E. M., Isokoski, K., van der Marel, N., & Linnartz, H. 2011, Mon. Not. R. Astron. Soc., 417, 2809
Cuppen, H. M., van Dishoeck, E. F., Herbst, E., & Tielens, A. G. G. M. 2009, Astron. Astrophys., 508, 275
Dartois, E., Cox, P., Roelfsema, P. R., et al. 1998, Astron. Astrophys., 338, L21
D'Hendecourt, L. B., Allamandola, L. J., & Greenberg, J. M. 1985, Astron. Astrophys., 152, 130
Draine, B. T. & Lee, H. M. 1984, Astrophys. J., 285, 89
Fayolle, E. C., Balfe, J., Loomis, R., et al. 2016, Astrophys. J. Lett., 816, L28
Fayolle, E. C., Bertin, M., Romanzin, C., et al. 2011, Astrophys. J. Lett., 739, L36
Fedoseev, G., Cuppen, H. M., Ioppolo, S., Lamberts, T., & Linnartz, H. 2015a, Mon. Not. R. Astron. Soc., 448, 1288
Fedoseev, G., Ioppolo, S., & Linnartz, H. 2015b, Mon. Not. R. Astron. Soc., 446, 449
Fillion, J.-H., Fayolle, E. C., Michaut, X., et al. 2014, Faraday Discussions, 168, 533
Fredon, A., Lamberts, T., & Cuppen, H. M. 2017, Astrophys. J., 849, 125
Fresneau, A., Danger, G., Rimola, A., et al. 2015, Molecular Astrophysics, 1, 1
Fuchs, G. W., Cuppen, H. M., Ioppolo, S., et al. 2009, Astron. Astrophys., 505, 629
Garrod, R. T., Vasyunin, A. I., Semenov, D. A., Wiebe, D. S., & Henning, T. 2009, Astrophys. J. Lett., 700, L43
Garrod, R. T., Wakelam, V., & Herbst, E. 2007, Astron. Astrophys., 467, 1103
Garrod, R. T., Widicus Weaver, S. L., & Herbst, E. 2008, Astrophys. J., 682, 283
Geballe, T. R. & Oka, T. 1996, Nature, 384, 334
Gerakines, P. A., Schutte, W. A., Greenberg, J. M., & van Dishoeck, E. F. 1995, Astron. Astrophys., 296, 810
Gibb, E. L., Whittet, D. C. B., Boogert, A. C. A., & Tielens, A. G. G. M. 2004, Astrophys. J. Suppl. Ser., 151, 35
Gibb, E. L., Whittet, D. C. B., Schutte, W. A., et al. 2000, Astrophys. J., 536, 347
Goesmann, F., Rosenbauer, H., Bredehöft, J. H., et al. 2015, Science, 349

Gottlieb, C. A. 1973, in Molecules in the Galactic Environment, 181
Gredel, R., Lepp, S., Dalgarno, A., & Herbst, E. 1989, Astrophys. J., 347, 289
Greenberg, J. M., Li, A., Mendoza-Gomez, C. X., et al. 1995, Astrophys. J. Lett., 455, L177
Henderson, B. L. & Gudipati, M. S. 2015, Astrophys. J., 800, 66
Henning, T. & Mutschke, H. 1997, Astron. Astrophys., 327, 743
Herbst. 2017, International Reviews in Physical Chemistry, 36, 287
Herbst, E. 1997, in IAU Symposium, Vol. 170, IAU Symposium, ed. W. B. Latter, S. J. E. Radford, P. R. Jewell, J. G. Mangum, & J. Bally, 71–78
Herbst, E. & Klemperer, W. 1973, Astrophys. J., 185, 505
Herbst, E. & van Dishoeck, E. F. 2009, Ann. Rev. Astron. Astrophys., 47, 427
Hidaka, H., Kouchi, A., & Watanabe, N. 2007, J. Chem. Phys., 126, 204707
Hidaka, H., Watanabe, M., Kouchi, A., & Watanabe, N. 2009, Astrophys. J., 702, 291
Hidaka, H., Watanabe, M., Kouchi, A., & Watanabe, N. 2011, Phys. Chem. Chem. Phys., 13, 15798
Hiraoka, K., Ohashi, N., Kihara, Y., et al. 1994, Chemical Physics Letters, 229, 408
Hollenberg, J. L. & Dows, D. A. 1961, J. Chem. Phys., 34, 1061
Hollis, J. M., Lovas, F. J., & Jewell, P. R. 2000, Astrophys. J. Lett., 540, L107
Hudgins, D. M., Sandford, S. A., Allamandola, L. J., & Tielens, A. G. G. M. 1993, Astrophys. J. Suppl. Ser., 86, 713
Ioppolo, S., Cuppen, H. M., Romanzin, C., van Dishoeck, E. F., & Linnartz, H. 2008, Astrophys. J., 686, 1474
Ioppolo, S., Fedoseev, G., Lamberts, T., Romanzin, C., & Linnartz, H. 2013, Review of Scientific Instruments, 84, 073112
Islam, F., Latimer, E. R., & Price, S. D. 2007, The Journal of chemical physics, 127, 064701
Jiménez-Serra, I., Vasyunin, A. I., Caselli, P., et al. 2016, Astrophys. J. Lett., 830, L6
Jørgensen, J. K., van der Wiel, M. H. D., Coutens, A., et al. 2016, Astron. Astrophys., 595, A117
Le Roy, L., Altwegg, K., Balsiger, H., et al. 2015, Astron. Astrophys., 583, A1
Ligterink, N. F. W., Paardekooper, D. M., Chuang, K.-J., et al. 2015, Astron. Astrophys., 584, A56
Linnartz, H., Ioppolo, S., & Fedoseev, G. 2015, International Reviews in Physical Chemistry, 34, 205
Maity, S., Kaiser, R. I., & Jones, B. M. 2015, Phys. Chem. Chem. Phys., 17, 3081
Marcelino, N., Cernicharo, J., Agúndez, M., et al. 2007, Astrophys. J. Lett., 665, L127
Martín-Doménech, R., Manzano-Santamaría, J., Muñoz Caro, G. M., et al. 2015, Astron. Astrophys., 584, A14
Meierhenrich, U. J. 2005, Angew. Chem. Int. Ed., 44, 5630
Mennella, V., Baratta, G. A., Esposito, A., Ferini, G., & Pendleton, Y. J. 2003, Astrophys. J., 587, 727
Millar, T. J., Bennett, A., & Herbst, E. 1989, Astrophys. J., 340, 906
Minissale, M., Moudens, A., Baouche, S., Chaabouni, H., & Dulieu, F. 2016, Mon. Not. R. Astron. Soc., 458, 2953
Miyauchi, N., Hidaka, H., Chigai, T., et al. 2008, Chemical Physics Letters, 456, 27
Modica, P. & Palumbo, M. E. 2010, Astron. Astrophys., 519, A22
Muñoz Caro, G. M., Jiménez-Escobar, A., Martín-Gago, J. Á., et al. 2010, Astron. Astrophys., 522, A108
Muñoz Caro, G. M., Meierhenrich, U. J., Schutte, W. A., et al. 2002, Nature, 416, 403
Nagaoka, A., Watanabe, N., & Kouchi, A. 2005, Astrophys. J. Lett., 624, L29
Nuevo, M., Auger, G., Blanot, D., & D'Hendecourt, L. 2008, Origins of Life and Evolution of the Biosphere, 38, 37
Öberg, K. I. 2016, Chemical Reviews, 116, 9631
Öberg, K. I., Boogert, A. C. A., Pontoppidan, K. M., et al. 2011a, Astrophys. J., 740, 109
Öberg, K. I., Bottinelli, S., Jørgensen, J. K., & van Dishoeck, E. F. 2010, Astrophys. J., 716, 825
Öberg, K. I., Fuchs, G. W., Awad, Z., et al. 2007, Astrophys. J. Lett., 662, L23
Öberg, K. I., Garrod, R. T., van Dishoeck, E. F., & Linnartz, H. 2009, Astron. Astrophys., 504, 891
Öberg, K. I., van der Marel, N., Kristensen, L. E., & van Dishoeck, E. F. 2011b, Astrophys. J., 740, 14
Paardekooper, D. M., Bossa, J.-B., & Linnartz, H. 2016a, Astron. Astrophys., 592, A67
Paardekooper, D. M., Fedoseev, G., Riedo, A., & Linnartz, H. 2016b, Astron. Astrophys., 596, A72

Pontoppidan, K. M. 2006, Astron. Astrophys., 453, L47
Pontoppidan, K. M., Boogert, A. C. A., Fraser, H. J., et al. 2008, Astrophys. J., 678, 1005
Pontoppidan, K. M., Fraser, H. J., Dartois, E., et al. 2003, Astron. Astrophys., 408, 981
Prasad, S. S. & Tarafdar, S. P. 1983, Astrophys. J., 267, 603
Ruaud, M., Wakelam, V., & Hersant, F. 2016, Mon. Not. R. Astron. Soc., 459, 3756
Rubin, R., Swenson Jr, G., Benson, R., Tigelaar, H., & Flygare, W. 1971, Astrophys. J., 169, L39
Schutte, W. A., Allamandola, L. J., & Sandford, S. A. 1993, Science, 259, 1143
Shen, C. J., Greenberg, J. M., Schutte, W. A., & van Dishoeck, E. F. 2004, Astron. Astrophys., 415, 203
Shu, F. H., Ruden, S. P., Lada, C. J., & Lizano, S. 1991, Astrophys. J. Lett., 370, L31
Solomon, P., Jefferts, K., Penzias, A., & Wilson, R. 1971, Astrophys. J., 168, L107
Taquet, V., Ceccarelli, C., & Kahane, C. 2012, Astron. Astrophys., 538, A42
Taquet, V., López-Sepulcre, A., Ceccarelli, C., et al. 2015, Astrophys. J., 804, 81
Terwisscha van Scheltinga, J., Ligterink, N. F. W., Boogert, A. C. A., van Dishoeck, E. F., & Linnartz, H. 2017, ArXiv e-prints
Tielens, A. G. G. M. & Allamandola, L. J. 1987, in Astrophysics and Space Science Library, Vol. 134, Interstellar Processes, ed. D. J. Hollenbach & H. A. Thronson, Jr., 397–469
Tielens, A. G. G. M. & Hagen, W. 1982, Astron. Astrophys., 114, 245
Tielens, A. G. G. M., Tokunaga, A. T., Geballe, T. R., & Baas, F. 1991, Astrophys. J., 381, 181
Tschersich, K. G. 2000, Journal of Applied Physics, 87, 2565
van Dishoeck, E. F. & Black, J. H. 1989, Astrophys. J., 340, 273
van Dishoeck, E. F. & Blake, G. A. 1998, Ann. Rev. Astron. Astrophys., 36, 317
Vastel, C., Ceccarelli, C., Lefloch, B., & Bachiller, R. 2014, Astrophys. J. Lett., 795, L2
Vasyunin, A. I. & Herbst, E. 2013a, Astrophys. J., 762, 86
Vasyunin, A. I. & Herbst, E. 2013b, Astrophys. J., 769, 34
Vidali, G. 2013, Chemical reviews, 113, 8762
Wakelam, V., Bron, E., Cazaux, S., et al. 2017, Molecular Astrophysics, 9, 1
Wakelam, V., Smith, I. W. M., Herbst, E., et al. 2010, Space Science Reviews, 156, 13
Walsh, C., Herbst, E., Nomura, H., Millar, T. J., & Weaver, S. W. 2014a, Faraday Discussions, 168, 389
Walsh, C., Millar, T. J., Nomura, H., et al. 2014b, Astron. Astrophys., 563, A33
Watanabe, N. & Kouchi, A. 2002, Astrophys. J. Lett., 571, L173
Watanabe, N., Mouri, O., Nagaoka, A., et al. 2007, Astrophys. J., 668, 1001
Westley, M. S., Baratta, G. A., & Baragiola, R. A. 1998, J. Chem. Phys., 108, 3321
Whittet, D. C. B., Bode, M. F., Longmore, A. J., et al. 1988, Mon. Not. R. Astron. Soc., 233, 321
Whittet, D. C. B., Schutte, W. A., Tielens, A. G. G. M., et al. 1996, Astron. Astrophys., 315, L357
Woods, P. M., Slater, B., Raza, Z., et al. 2013, Astrophys. J., 777, 90
Wootten, A. 1987, in IAU Symposium, Vol. 120, Astrochemistry, ed. M. S. Vardya & S. P. Tarafdar, 311–318
Zhitnikov, R. A. & Dmitriev, Y. A. 2002, Astron. Astrophys., 386, 1129